Quantum control in two-dimensional Fourier-transform spectroscopy

Jongseok Lim, Han-gyeol Lee, Sangkyung Lee, and Jaewook Ahn
Department of Physics, KAIST, Daejeon 305-701, Korea
(Received 2 September 2010; published 28 July 2011)

We present a method that harnesses coherent control capability to two-dimensional Fourier-transform optical spectroscopy. For this, three ultrashort laser pulses are individually shaped to prepare and control the quantum interference involved in two-photon interexcited-state transitions of a V-type quantum system. In experiments performed with atomic rubidium, quantum control for the enhancement and reduction of the $5P_{1/2} \rightarrow 5P_{3/2}$ transition was successfully tested in which the engineered transitions were distinguishably extracted in the presence of dominant one-photon transitions.

DOI: 10.1103/PhysRevA.84.013425 PACS number(s): 32.80.Qk, 32.80.Wr, 42.50.Md, 42.65.Re

I. INTRODUCTION

One of the fundamental goals in chemical physics and biophysics is to understand how molecular structural dynamics, which are often manifested in interexcited-electronic-state transitions, proceed during chemical reactions or interactions with light and what the implications are for known chemical and biological processes [1]. The best known tool is two-dimensional nuclear magnetic resonance (2D NMR) spectroscopy [2], which is especially useful for the detailed analysis of molecular structures. However, 2D NMR is primarily limited to probing relatively small molecular systems, and structural evolution occurring in the subpicosecond time scale is too fast for 2D NMR to resolve. Alternatively, 2D Fourier-transform optical spectroscopy (2D FTOS) [3,4], an optical extension of 2D NMR, has recently been developed to probe femtosecond electronic and vibrational dynamics. It can be applied to molecules as large as small proteins and provides ultrafast time resolution, which is crucial to understand reaction dynamics and energy transfer processes [5].

In this paper, we present a method that harnesses the ability to control the evolution of quantum systems with 2D FTOS. Quantum mechanical control of matter, known as quantum control or coherent control, utilizes programmed light forms and has become a general scientific subject of extreme interest because of its unprecedented control capability over the dynamics of atoms and molecules [6–8]. In particular, with the recent development of the ultrafast optical technique of shaping laser pulses, termed ultrafast pulse shaping, coherent control has been demonstrated in a variety of material substances extending from atoms and molecules to solid-state and biological systems [9–13]. However, not many analytical solutions are known despite great efforts to describe the shaped-pulse control of transition probabilities even in simple atomic systems [14–18]. This previous research is restricted to the transitions from a ground state to excited states, mainly due to the limitation of the detection techniques. In ladder-type systems, for example, the transition probability can be easily measured by detecting the target excited-state fluorescence. On the other hand, in a V-type system, especially if we consider the transition from one of the excited states to the other, the interexcited-state transition cannot be measured straightforwardly and thus is difficult to control [19,20]. The target excited-state population in this case is coherently mixed with and is difficult to separate from the dominant one-photon transitions from the ground state. This difficulty of distinguishing the interexcited-state transition from the others is overcome by using quantum coherence of the system with 2D FTOS.

Here, we describe an experimental demonstration of coherent control of transitions between two excited states in a V-type system. To do this, we adopt the recently devised three-pulse coherent control scheme in a 2D FTOS setting [21]. The target transition probability can be retrieved from distinct 2D Fourier-transform (FT) spectral peaks that are inherent to their transition pathways, and thereby, the controlled transition-probability amplitude is obtained. By shaping one of the three laser pulses used in 2D FTOS, we selectively turn on and off the $5P_{1/2}$-$5P_{3/2}$ transition of atomic rubidium (Rb). Furthermore, by engineering the quantum interference among the involved transition paths, a net transition increase of 300% relative to the Fourier-transform-limited (FTL)-pulse case is achieved.

II. THEORETICAL MODEL

We consider a three-pulse interaction with a V-type quantum system in which the second pulse is the control pulse and the first and third pulses are used to retrieve the controlled second-pulse interaction in a 2D FTOS setting [22]. The quantum system under consideration comprises one ground state $|g\rangle$ and two adjacent excited states $|a\rangle$ and $|b\rangle$ ($5S_{1/2}$, $5P_{1/2}$, and $5P_{3/2}$ respectively in Rb). For the quantum system initially in the ground state, the wave function after the first-pulse interaction is

$$|\psi(0+)\rangle = |g\rangle + \alpha_{ag}^{(1)}|a\rangle + \alpha_{bg}^{(1)}|b\rangle, \tag{1}$$

where $\alpha_{ij}^{(1)}$ denotes the first-order transition-probability amplitude from state $|j\rangle$ to state $|i\rangle$, in the weak-field interaction regime. After a time delay τ_1, the second pulse interacts and the wave function becomes

$$|\psi(\tau_1)\rangle = \begin{pmatrix} 1 & \beta_{ag}^{(1)*} e^{-i\Delta\omega_{ag}\tau_1} & \beta_{bg}^{(1)*} e^{-i\Delta\omega_{bg}\tau_1} \\ \beta_{ag}^{(1)} e^{i\Delta\omega_{ag}\tau_1} & 1 & \beta_{ab}^{(2)} e^{i(\Delta\omega_{ag}-\Delta\omega_{bg})\tau_1} \\ \beta_{bg}^{(1)} e^{i\Delta\omega_{bg}\tau_1} & \beta_{ba}^{(2)} e^{-i(\Delta\omega_{ag}-\Delta\omega_{bg})\tau_1} & 1 \end{pmatrix} \times |\psi(0+)\rangle, \tag{2}$$

where $\Delta\omega_{ij} = \omega_{ij} - \omega_0$ and $\beta^{(1,2)}$ denote the first- and second-order transition-probability amplitudes, respectively, for the second pulse. The matrix (evolution operator) is written in terms of three states $\{|g\rangle,|a\rangle,|b\rangle\}$, and the rotating wave approximation is used. Likewise, after the third pulse with the time delay τ_2 with respect to the second pulse, the final wave function is given by

$$|\psi(\tau_1+\tau_2)\rangle = \begin{pmatrix} 1 & \gamma_{ag}^{(1)*} e^{-i\Delta\omega_{ag}(\tau_1+\tau_2)} & \gamma_{bg}^{(1)*} e^{-i\Delta\omega_{bg}(\tau_1+\tau_2)} \\ \gamma_{ag}^{(1)} e^{i\Delta\omega_{ag}(\tau_1+\tau_2)} & 1 & \gamma_{ab}^{(2)} e^{i(\Delta\omega_{ag}-\Delta\omega_{bg})(\tau_1+\tau_2)} \\ \gamma_{bg}^{(1)} e^{i\Delta\omega_{bg}(\tau_1+\tau_2)} & \gamma_{ba}^{(2)} e^{-i(\Delta\omega_{ag}-\Delta\omega_{bg})(\tau_1+\tau_2)} & 1 \end{pmatrix} |\psi(\tau_1)\rangle, \tag{3}$$

where $\gamma^{(1,2)}$ denote the transition-probability amplitudes for the third pulse.

After all three pulsed interactions, the probability of the state $|b\rangle$, $P_b = |\langle b|\psi\rangle|^2$, is given as a function of the two interpulse delays as

$$P_b(\tau_1,\tau_2) = \left|\alpha_{bg}^{(1)}\right|^2 + \left|\beta_{bg}^{(1)}\right|^2 + \left|\gamma_{bg}^{(1)}\right|^2 + \cdots + \alpha_{ag}^{(1)*}\beta_{ba}^{(2)*}\gamma_{bg}^{(1)} e^{i(\Delta\omega_{ag}\tau_1+\Delta\omega_{bg}\tau_2)} + \cdots, \tag{4}$$

where the term $\alpha_{ag}^{(1)*}\beta_{ba}^{(2)*}\gamma_{bg}^{(1)}\exp(i\Delta\omega_{ag}\tau_1 + i\Delta\omega_{bg}\tau_2)$ results from the quantum interference between the two transitions $\alpha_{ag}^{(1)*}\beta_{ba}^{(2)*}$ and $\gamma_{bg}^{(1)}$, respectively representing $|g\rangle \to |a\rangle \to |b\rangle$ and $|g\rangle \to |b\rangle$. The coefficient $\alpha_{ag}^{(1)*}\beta_{ba}^{(2)*}\gamma_{bg}^{(1)}$ is retrieved from the spectral peak located at $(\omega_1,\omega_2) = (\Delta\omega_{ag},\Delta\omega_{bg})$ of the 2D FT spectrum of P_b, i.e.,

$$\alpha_{ag}^{(1)*}\beta_{ba}^{(2)*}\gamma_{bg}^{(1)} = S(\omega_{ag}-\omega_0,\omega_{bg}-\omega_0), \tag{5}$$

where $S(\omega_1,\omega_2)$ is defined by

$$S(\omega_1,\omega_2) = \int\int P_b(\tau_1,\tau_2) e^{-i(\omega_1\tau_1+\omega_2\tau_2)} d\tau_1 d\tau_2. \tag{6}$$

Therefore, aside from the constant $\alpha_{ag}^{(1)*}\gamma_{bg}^{(1)}$, the controlled second-pulse interaction $\beta_{ba}^{(2)*}$ (or the two-photon coherent control from $|a\rangle$ to $|b\rangle$) is retrieved from the 2D FTOS measurement [21].

III. EXPERIMENTAL DESCRIPTION

To demonstrate coherent control in the 2D FTOS setting, experiments were performed in atomic ^{87}Rb vapor at room temperature. We used a homemade Ti:sapphire laser amplifier system producing 35 fs pulses (FTL case) at a repetition rate of 1 kHz, delivered in a beam of 3 mm diameter. An actively controlled acousto-optic programmable dispersive filter (AOPDF) was installed between the gain media of the laser amplifier and the pulse compressor to generate an independently shaped three-pulse sequence from one pulse of 1 kHz pulse train (Fig. 1). The shaped pulses had 4 μJ of energy each, which interacted with Rb in the weak-field regime with a maximum intensity of 2.3×10^8 W/cm^2. The interpulse delays τ_1 and τ_2, or the time intervals between the first and second pulses and between the second and third pulses, respectively, were varied from 0 to 1638 fs in 26 fs steps. The wavelength of each pulse was centered at 800 nm with a bandwidth of 26 nm full width at half maximum (FWHM), which covered the $5S_{1/2}$-$5P_{1/2}$ D_1 (794.7 nm) and $5S_{1/2}$-$5P_{3/2}$ D_2 (780 nm) transitions of Rb, and the weak transitions to the $5D$ state were ignored. After the three pulses were applied, the spectrally filtered (3 nm bandwidth at

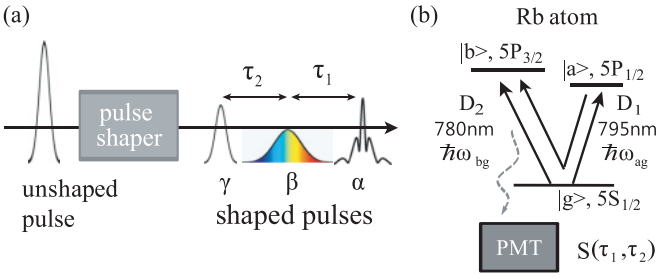

FIG. 1. (Color online) (a) Schematic diagram of the pulse-shaping scenario. The first pulse has a spectral hole around the D_2 ($|g\rangle \to |b\rangle$) transition, and the second pulse is shaped to control the $|a\rangle \to |b\rangle$ transition. The third pulse is unshaped. (b) Energy level diagram of atomic rubidium.

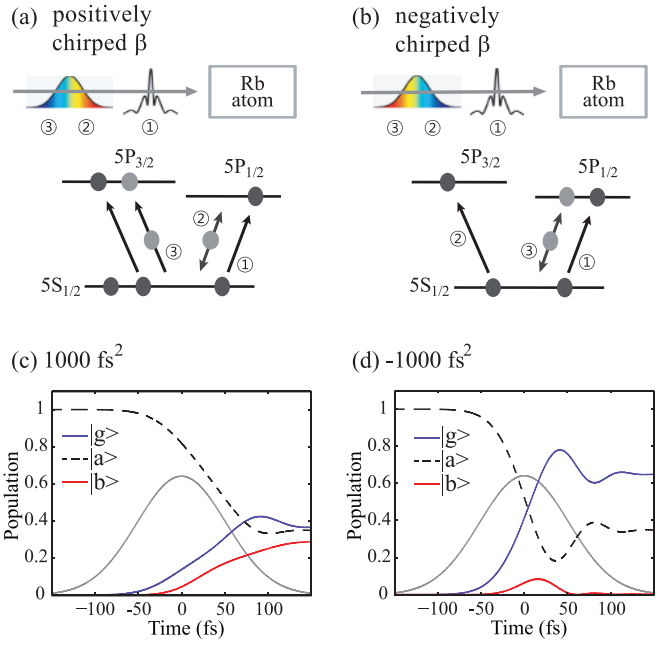

FIG. 2. (Color online) Chirped pulse control of $|a\rangle \to |b\rangle$ transition: (a) positive chirp case; (b) negative chirp case. Depending on the chirp sign, the sequence of D_1 and D_2 transitions is time reversed. The circled numbers indicate the transition sequence. (c),(d) Numerical calculation of the time evolution of $5S_{1/2}$ (blue line), $5P_{1/2}$ (dashed line), and $5S_{3/2}$ (red line) populations as well as the field envelope (solid black line), corresponding to (a) and (b), respectively.

780 nm for D_2) fluorescence signal $S(\tau_1,\tau_2)$ was recorded using a photomultiplier tube (PMT).

IV. RESULTS AND DISCUSSION

A. Linear chirp control

For the first experiment, we demonstrated selective turn-on and turn-off of the target transition from $|a\rangle$ to $|b\rangle$ by applying a linear chirp to the control pulse (the second pulse). The intuitive ordering of frequencies in the pulse, for an effective transfer, is that the atoms are first driven from $|a\rangle$ to $|g\rangle$ (resonant at 794.7 nm) with the red-detuned frequency components and then from $|g\rangle$ to $|b\rangle$ (resonant at 780 nm) with the blue-detuned components. So, as Fig. 2(a) shows, a positively chirped control pulse brings the atoms in $|a\rangle$, which are initially excited by the first pulse, down to $|g\rangle$ and then back up to the $|b\rangle$ state, because the low-energy part of the spectrum arrives ahead of time compared to the high-energy part in this case. On the other hand, the spectrotemporal correlation is reversed in a negatively chirped pulse, and the other case, shown in Fig. 2(b), leaves the $|a\rangle$ and $|b\rangle$ states uncoupled. So the chirp of the control pulse determines the strength of the $|a\rangle \rightarrow |b\rangle$ transition.

This control scenario was first checked by numerical simulation. The results, shown in Figs. 2(c) and 2(d), confirm that the state populations of the $5S_{1/2}$ (blue line), $5P_{1/2}$ (dashed line), and $5S_{3/2}$ (red line) states, for the linear chirp values of (c) -1000 fs^2 and (d) -1000 fs^2, respectively, evolve in time as predicted. The initial population was fixed as $(5S_{1/2},5P_{1/2},5P_{3/2}) = (0,1,0)$, and a pulse energy about fivefold that of the experimental pulse was used in order to illustrate the transition behaviors more clearly. Note that the behavior with smaller pulse energies is less dramatic but remains in general accordance.

Figure 3 shows the experimental results. The 2D time-domain measurements of $P_b(\tau_1,\tau_2)$, which are obtained for the various linear chirps of the second pulse, and their 2D FT spectra $S(\omega_1,\omega_2)$ are shown in Figs. 3(a)–3(e). The suppression of the $|a\rangle \rightarrow |b\rangle$ transition is clearly observed for the negatively chirped pulses and the enhancement for the positively chirped pulses. So the chirp control of the $5P_{1/2} \rightarrow 5P_{3/2}$ transition of Rb was successfully demonstrated. For a chirped laser pulse given by,

$$E(\omega) = E_0 \exp\left[-\frac{(\omega-\omega_0)^2}{\Delta\omega^2} + i\frac{a_2}{2}(\omega-\omega_0)^2\right], \quad (7)$$

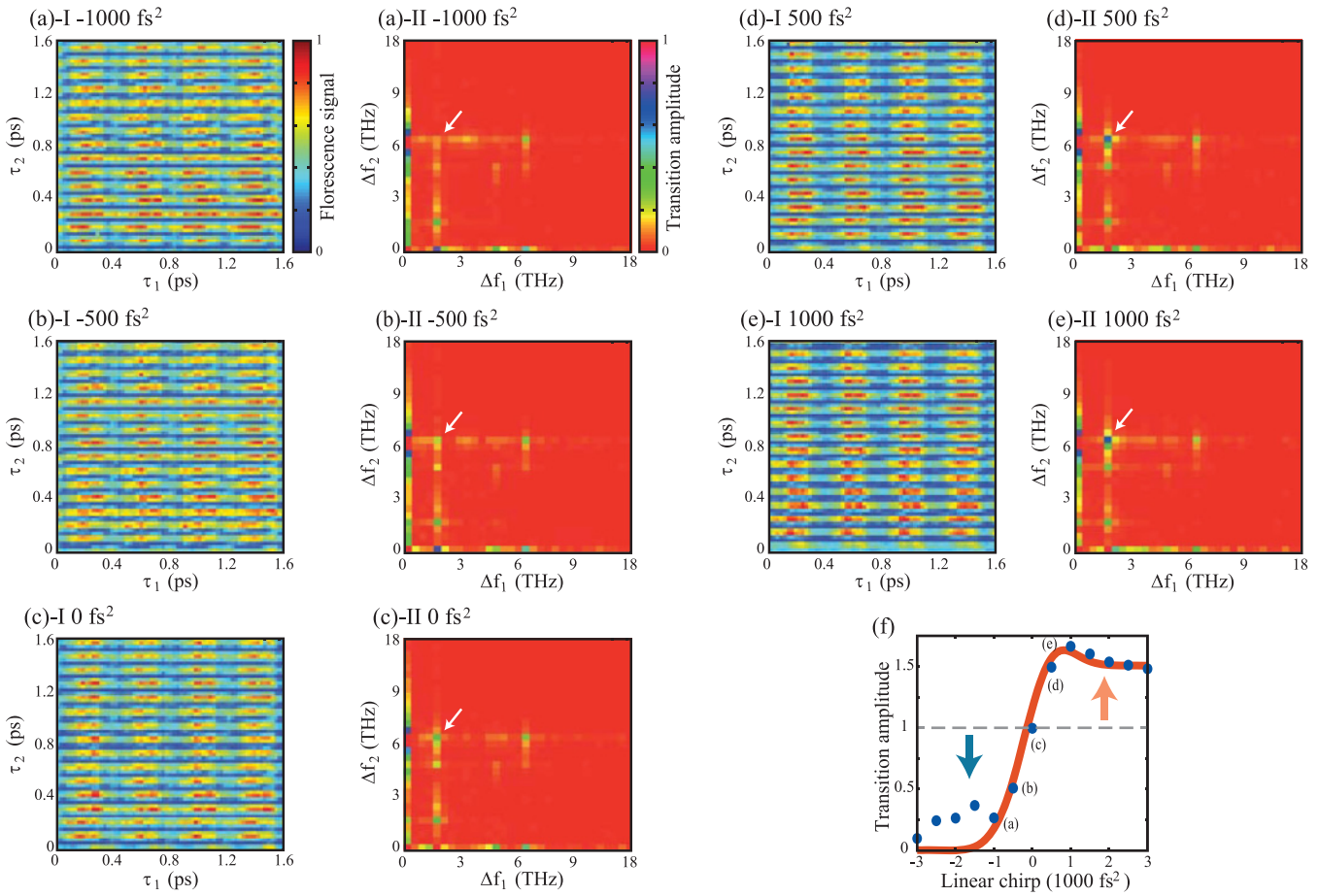

FIG. 3. (Color online) (a)–(e) Experimental results of the 2D measurement of P_b as a function of τ_1 and τ_2 (column I) and their 2D FT spectra $S(\omega_1, \omega_2)$ (column II) for shaped pulses with five different chirp coefficients: (a) -1000 fs^2, (b) -500 fs^2, (c) 0 fs^2, (d) 500 fs^2, and (e) 1000 fs^2. The peaks at $(\omega_{ag}-\omega_0, \omega_{bg}-\omega_0)$ are marked by white arrows which represent the target two-photon process $5P_{1/2} \rightarrow 5P_{3/2}$. (f) Extracted peak amplitudes at $(\omega_{ag}-\omega_0, \omega_{bg}-\omega_0)$ plotted as a function of chirp of the second pulses (circles) are compared with the numerical calculation of $\beta^{(2)}_{ba}$ (line).

where ω_0 and $\Delta\omega$ are the laser frequency and the spectral bandwidth, respectively, and a_2 is the linear chirp rate, second-order perturbation theory predicts that the two-photon transition-probability amplitude $c_{ba}^{(2)}$ can be obtained as

$$\beta_{ba}^{(2)} \propto 1 + \mathrm{Erf}\left[\frac{\Delta\omega(\omega_{bg}-\omega_{ag})}{\sqrt{8}}a_2 + i\frac{\omega_{bg}+\omega_{ag}-2\omega_0}{\sqrt{2}\Delta\omega}\right], \tag{8}$$

where ω_{nm} is the resonance frequency of the transition from $|m\rangle$ to $|n\rangle$ and $\mathrm{Erf}(x)$ is the Gaussian error function [23]. Note that the error function in Eq. (8) approximates a sign function for a sufficiently large a_2 [i.e., $|a_2| \gg 1/\Delta\omega(\omega_{bg}-\omega_{ag})$]. Figure 3(f) shows the agreement of the measured transition-probability amplitudes obtained for linear chirps $[-3,3] \times 10^3$ fs^2 with 500 fs^2 and the numerical simulation based on Eq. (8).

B. Spectral phase shaping

The second experiment aims for further enhancement of the $|a\rangle \rightarrow |b\rangle$ transition by applying a general phase function to the control pulse. We start by considering the two-photon transition-probability amplitude written in the spectral domain given as [21]

$$\beta_{ba}^{(2)} = \frac{\mu_{ga}\mu_{gb}}{\hbar^2}\left[-\pi E^*(\omega_{ag})E(\omega_{bg}) - i\mathrm{P}\int_{-\infty}^{\infty} d\omega \frac{E^*(\omega)E(\omega_{ba}+\omega)}{\omega_{ag}-\omega}\right], \tag{9}$$

where μ_{nm} is a dipole moment matrix element, $E(\omega)$ the inverse Fourier transform of the electric field, and P the Cauchy principal value. For a laser pulse having the spectral components all in phase, the resonant contribution is real [the first term in Eq. (9)], and the two nonresonant contributions (the second term) below and above the resonance frequency ω_{ag} are both imaginary but out of phase with respect to each other. Hence, the three components, the resonant part and the upper and lower nonresonant parts, add up to the total transition $\beta_{ba}^{(2)}$, and $\beta_{ba}^{(2)}$ can be enhanced by engineering the interference among them. By encoding a constant block phase ϕ_b over a block spectral region $[\omega_{ag},\omega_{ag}+\omega_{ba}]$, the interference of the three transition components of the dominant spectral region can be altered. The transition probability amplitude c_{ba} in Eq. (9) can be disassembled as

$$\beta_{ba}^{(2)} = i\frac{\mu_{ga}\mu_{gb}}{\hbar^2}\left[i\pi E^*(\omega_{ag})E(\omega_{bg}) - e^{i\phi_b}\int_{\omega_{ag}-\omega_{ba}}^{\omega_{ag}} \frac{E^*(\omega)E(\omega_{ba}+\omega)}{|\omega_{ag}-\omega|}d\omega + e^{-i\phi_b}\int_{\omega_{ag}}^{\omega_{ag}+\omega_{ba}} \frac{E^*(\omega)E(\omega_{ba}+\omega)}{|\omega_{ag}-\omega|}d\omega\right], \tag{10}$$

where the first, second, and third terms correspond to A, B, and C in the phase diagram in the upper left inset of Fig. 4(a).

In our experiment, transition-amplitude absolutes are given by $|A|:|B|:|C| = 1:2.8:1.6$. Figure 4(a) shows the measured net transition-probability amplitudes as a function of ϕ_b. The dots are experimental results, and the black dashed line is the theoretical calculation based on Eq. (9). The spectral phase function was smeared by 0.2 nm in the experiment, and inclusion of this consideration (shown with the solid line) gives a more accurate fit to the experimental results. Two local maxima are expected from Eq. (10), one at $\phi_b = \pi/2$ and the other at $\phi_b = 3\pi/2$. As shown in Figs. 4(b)–4(d), the three transition components A, B, and C, interfere either constructively or destructively with each other. For example, in Fig. 4(d), the three components are all in phase, maximizing the quantum interference. In such conditions, the transition-probability amplitude is tripled compared to the FTL case.

C. Spectral amplitude shaping

Alternatively, spectral amplitude shaping of the control pulse can be considered to enhance the given two-photon transition. For example, among the components in Eq. (10), the smaller nonresonant transition component C can be removed. For this, the nonresonant component of the transition-probability amplitude [the second term of Eq. (9)] can be rephrased as

$$\beta_{ba}^{(2)nr} = \frac{\mu_{ga}\mu_{gb}}{i\hbar^2}\left[\int_{\infty}^{\omega_{bg}} \frac{E^*(\omega-\omega_{ba})E(\omega)}{|\omega_{bg}-\omega|}d\omega - \int_{\omega_{bg}}^{\omega_{cut}} \frac{E^*(\omega-\omega_{ba})E(\omega)}{|\omega_{bg}-\omega|}d\omega\right], \tag{11}$$

where the spectrum below ω_{cut} is eliminated [the second term in Eq. (9)] as depicted in the inset of Fig. 5. In the final experiment, we utilized the spectral amplitude block above the cutoff frequency (ω_{cut}) in the second pulse (the spectral phase was unchanged.) The tested transition-probability amplitudes

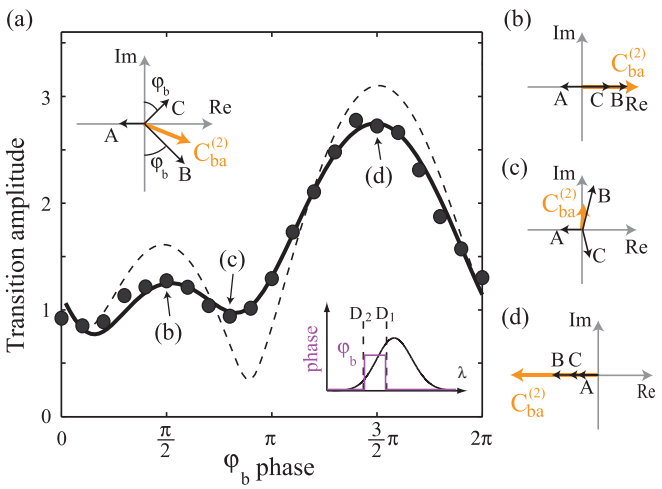

FIG. 4. (Color online) (a) Experimental and theoretical results for the quantum interference engineering. Dots, measured transition-amplitude absolutes; dashed line, numerical calculation based on Eq. (9); solid line, numerical calculation considering the spectrally smeared phase (see the text). Inset, upper left: The phase diagram for the three transition components in Eq. (10). Inset, lower right: The laser spectrum in the block spectral phase in which the block spectral phase ϕ_b represents the relative phase of the spectral region in $[\omega_{ag},\omega_{bg}]$ with respect to the other. (b)–(d) The phase diagrams for the maximal (b),(d) and minimal (c) quantum interference conditions.

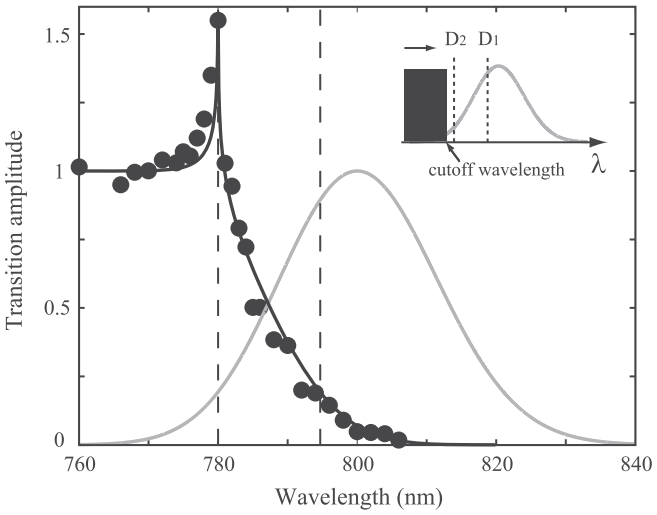

FIG. 5. Coherent enhancement experiment of the $5P_{1/2} \rightarrow 5P_{3/2}$ transition of Rb by spectral amplitude shaping. The measured transition-probability amplitudes, normalized to the full spectrum limit (dots), are plotted along with the calculated data (dark line) as a function of the cutoff wavelength. The laser spectrum is shown by the gray line. The inset illustrates the spectral shape used in the experiment. The dashed lines are the D_1 and D_2 resonant wavelengths.

$c_{ba}^{(2)}$ are retrieved from the 2D FT spectra $S(\omega_1,\omega_2)$ as a function of $\omega_{\rm cut}$. The experimental result is shown in dots in Fig. 5, and the theoretical results (black solid line) are calculated using Eq. (9). The normalized laser spectrum is shown as a gray solid line, and the resonance wavelengths are denoted by black dashed lines in Fig. 5. As the cutoff wavelength $\lambda_{\rm cut}$ $(=2\pi/\omega_{\rm cut})$ approaches the resonance wavelength λ_{bg} from the short-wavelength end, the second term of $\beta_{ba}^{(2)nr}$, or C in Eq. (10), becomes smaller and, therefore, the target $|a\rangle \rightarrow |b\rangle$ transition is enhanced. The two-photon transition $\beta_{ba}^{(2)}$ is maximally enhanced, for $\lambda_{\rm cut} = \lambda_{bg}$, by 60% compared to the full spectrum limit.

V. CONCLUSIONS

In conclusion, we have demonstrated a combination of two powerful techniques, the coherent control of pulse shaping and 2D FTOS. For this, we utilized three individually shaped optical short pulses in a 2D FTOS scheme, and the two-photon interexcited-state transition of a V-type quantum system was retrieved in the presence of dominant one-photon transitions. In the coherently controlled 2D FTOS experiments performed on Rb atoms, linear spectral chirp was used to turn on and off the $5P_{1/2} \rightarrow 5P_{3/2}$ transition. Furthermore, experiments for quantum interference engineering revealed that the target transition strength is tripled in spectral phase shaping and enhanced by 60% in spectral amplitude shaping. We hope that the devised coherent control for excited-state transitions will become useful in untangling the unknown nature of chemical and biological reaction processes.

ACKNOWLEDGMENTS

This research was supported by Basic Science Research and Mid-career Researcher Programs through the National Research Foundation of Korea (NRF) funded by the Ministry of Education, Science and Technology (Grant Nos. 2009-0090843 and 2010-0013899).

[1] P. Tian, D. Keusters, Y. Suzaki, and W. S. Warren, Science **300**, 1553 (2003).
[2] G. E. Martin and A. S. Zekter, *Two-Dimensional NMR Methods for Establishing Molecular Connectivity* (Wiley-VCH, New York, 1988).
[3] D. M. Jonas, Annu. Rev. Phys. Chem. **54**, 425 (2003).
[4] K. W. Stone, K. Gundogdu, D. B. Turner, X. Li, S. T. Cundiff, and K. A. Nelson, Science **324**, 1169 (2009).
[5] T. Brixner, J. Stenger, H. M. Vaswani, M. Cho, R. E. Blankenship, and G. R. Fleming, Nature (London) **434**, 625 (2005).
[6] K. Bergmann, H. Theuer, and B. W. Shore, Rev. Mod. Phys. **70**, 1003 (1998).
[7] M. Shapiro and P. Brumer, *Principles of the Quantum Control of Molecular Processes* (Wiley, New York, 2003).
[8] D. J. Tanner and S. A. Rice, J. Chem. Phys. **83**, 5013 (1985).
[9] E. D. Potter, J. L. Herek, S. Pedersen, Q. Liu, and A. H. Zewail, Nature (London) **355**, 66 (1992).
[10] L. Costa, M. Betz, M. Spasenovic, A. D. Bristow, and H. M. van Driel, Nature Phys. **3**, 632 (2007).
[11] J. P. Ogilvie, D. Debarre, X. Solinas, J.-L. Martin, E. Beaurepaire, and M. Joffre, Opt. Express **14**, 759 (2006).
[12] A. Assion, T. Baumert, J. Helbing, V. Seyfried, and G. Gerber, Chem. Phys. Lett. **259**, 488 (1996).
[13] T. C. Weinacht, J. Ahn, and P. H. Bucksbaum, Nature (London) **397**, 233 (1999).
[14] N. Dudovich, B. Dayan, S. M. Gallagher Faeder, and Y. Silberberg, Phys. Rev. Lett. **86**, 47 (2001).
[15] S. D. Clow, C. Trallero-Herrero, T. Bergeman, and T. Weinacht, Phys. Rev. Lett. **100**, 233603 (2008).
[16] M. C. Stowe, A. Peer, and J. Ye, Phys. Rev. Lett. **100**, 203001 (2008).
[17] S. Lee, J. Lim, J. Ahn, V. Hakobyan, and S. Guerin, Phys. Rev. A **82**, 023408 (2010).
[18] A. M. Weiner, D. E. Leaird, G. P. Wiederrecht, and K. A. Nelson, Science **247**, 1317 (1990).
[19] L. Yang, I. V. Schweigert, S. T. Cundiff, and S. Mukamel, Phys. Rev. B **75**, 125302 (2007).
[20] L. Yang, T. Zhang, A. D. Bristow, S. T. Cundiff, and S. Mukamel, J. Chem. Phys. **129**, 234711 (2008).
[21] J. Lim, H. G. Lee, J. U. Kim, S. Lee, and J. Ahn, Phys. Rev. A **83**, 053429 (2011).
[22] A more general description for the three-pulse coherent control of a V-type system is introduced in the Appendix of Ref. [21]. Section II summarizes the results of particular relevance in the context of the present experiments.
[23] W. J. Cody, Math. Comput. **23**, 631 (1969).